Vacuum ultraviolet excitation and emission properties of Pr^{3+} and Ce^{3+} in MSO_4 (M=Ba, Sr, and Ca) and predicting quantum splitting by Pr^{3+} in oxides and fluorides

E. van der Kolk, P. Dorenbos, A. P. Vink, R. C. Perego, and C. W. E. van Eijk
Interfaculty Reactor Institute, Delft University of Technology, Mekelweg 15, 2629 JB Delft, The Netherlands

A. R. Lakshmanan
Health and Safety Department, Indira Ghandi Centre for Atomic Research, Kalpakkam, India

(Received 26 April 2001; published 29 October 2001)

The excitation and emission properties of Pr^{3+} and Ce^{3+} doped MSO_4 ($M^{2+}=Ca^{2+}$, Sr^{2+}, and Ba^{2+}) were investigated at 293 and 10 K. The lowest $5d$ level in $CaSO_4:Pr^{3+}$ is located below the $4f^2[^1S_0]$ level resulting in allowed $4f5d\rightarrow4f^2$ transitions. In $BaSO_4$ and $SrSO_4$ the lowest $5d$ level appears above the $^1S_0$ level and $4f^2[^1S_0]\rightarrow4f^2$ emission is observed. However, also $4f5d\rightarrow4f^2$ emission occurs, suggesting the presence of two different Pr centers. The unusual temperature dependence of the emission, points, however, to a thermal excitation process from the $^1S_0$ state to the $4f5d$ states involving only one site. The internal quantum efficiency of the $^3P_0$ and $^1D_2$ emission in $BaSO_4$ is estimated to be 0.1 and 1%, respectively. It will be demonstrated that under host lattice excitation part of the energy is transferred to $4f^2$ states with lower energy than the $^1S_0$ or the $4f5d$ states. The possibility for quantum splitting to occur in Pr^{3+} doped oxides and fluorides will be discussed. Trends observed in the interaction between the crystal field and the $5d$ electron of Ce^{3+}, will be applied to predict the energy of the $4f5d$ states of Pr^{3+}.

DOI: 10.1103/PhysRevB.64.195129 PACS number(s): 78.55.Hx, 71.70.Ch, 71.55.−i, 71.35.Aa

I. INTRODUCTION

The luminescence of the Pr^{3+} ion doped in inorganic compounds has been investigated thoroughly in relation with several applications. Laser action from the $^3P_0$ and $^1D_2$ states[1,2] in the visible part of the spectrum, or from the $^1G_4$ state in the infrared part[3–5] has been described in detail and is utilized in for example fiber optical communication. The red $^1D_2$ emission around 600 nm has proven useful as a primary color in field emission display (FED) devices.[6,7] Emission from the opposite parity $4f5d$ state results in fast ns ultraviolet (UV) emission, useful for scintillator applications[8,9] or tunable UV lasers.[10–12]

This work deals mainly with emission from the $^1S_0$ state, which is the highest energy $4f^2$ state of Pr^{3+}. After the $^1S_0$ state is populated, the ground state can be reached by a two step radiative process involving the transitions $^1S_0\rightarrow{}^1I_6,{}^3P_J$ followed by $^3P_0\rightarrow{}^3F_J,{}^3H_J$ or $^1S_0\rightarrow{}^1D_2$ followed by $^1D_2\rightarrow{}^3H_J$, see Fig. 1(a). This photon cascade emission (PCE) or quantum splitting phenomenon, demonstrated in the fluorides YF_3, LaF_3, and $NaYF_4$ (Refs. 13–15) and in the oxides $SrAl_{12}O_{19}$,[16] $LaMgB_5O_{10}$,[17] and LaB_3O_6,[18] can be useful in plasma display panels (PDP's) and Hg-free lighting tubes, in which phosphors are excited by the vacuum ultraviolet (VUV) emission (150–180 nm) from a discharge in a noble gas mixture containing Xe.[19] The high energy of the VUV photons (7–8 eV), relative to the visible photons (2–3 eV), results in an inefficient emissive device, but allows at the same time for a possible emission of two visible photons for each absorbed VUV photon, resulting in a luminescent material with an internal quantum efficiency larger than unity.

The energies of the $4f5d$ states are of crucial importance for many type of applications involving the $4f^{n-1}5d$ states of trivalent lanthanides. In order to observe PCE by Pr^{3+} it is required that the $4f5d$ states of Pr^{3+} have an energy higher than the $^1S_0$ state since otherwise $4f5d\rightarrow4f^2$ emission is observed instead. This is illustrated in Fig. 1(b). Clearly, methods to predict $5d$-level energies will be very helpful in selecting candidate host materials for Pr^{3+}.

Recently, Dorenbos collected data on $4f^{n-1}5d$-level en-

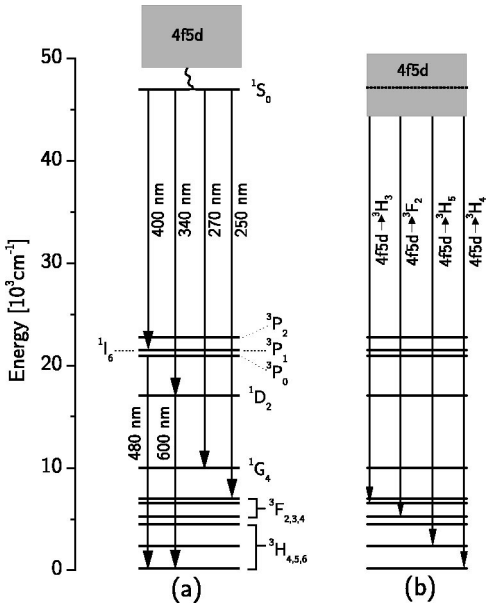

FIG. 1. Schematic representation of the excited states of Pr^{3+}. The most probable radiative transitions are indicated by the vertical arrows for the situation where the lowest $4f5d$ state has a higher energy (a) or a lower energy (b) than the $4f^2[^1S_0]$ state.

ergies of Ln^{3+} ions in a wide variety of inorganic compounds.[20,21] The lowest $5d$-level may shift downwards by as much as 30 000 cm^{-1} from the free ion value due to the interaction of the $5d$ electron with the crystal field. To understand this wide variation, the relation between the energy of $5d$ levels and the crystalline environment was systematically investigated in Refs. 22–25.

This work reports on the excitation and emission properties of Pr^{3+} and Ce^{3+} doped MSO_4 ($M^{2+}=Ca^{2+}$, Sr^{2+}, and Ba^{2+}) in the VUV to visible spectral range. The observed $^1S_0$ emission, the luminescence quantum efficiency of the $^3P_0$ and $^1D_2$ states as well as the energy transfer from the host lattice to the Pr^{3+} ion is described and discussed. Furthermore the shape of the excitation spectra of Ce^{3+} and Pr^{3+} luminescence in the same host crystals are compared with each other.

This work also addresses the possibility to observe quantum splitting by Pr^{3+} in oxides and fluorides. Relationships between $5d$-level energies and crystalline environment known for Ce^{3+}, will be applied to $4f5d$ states of Pr^{3+}. It appears that quantum splitting is possible in oxides that contain ionic complexes (SO_4^{2-}, PO_4^{3-}, BO_3^{3-}, and SiO_4^{4-}) provided specific conditions are met. Conditions are particularly favorable in the sulfates with large cations as in $SrSO_4$ and $BaSO_4$.

This paper is organized as follows. We will start with a general description of the physical and chemical properties of the lanthanides and the host crystal that determine the energy of the lowest $4f^{n-1}5d$ level of the trivalent lanthanides in inorganic compounds. From that our choice to study the alkaline earth sulfates as host for Pr^{3+} will be motivated. Next the experimental results will be presented, and finally we will explore the prospects to find other host materials that, when doped with Pr^{3+}, may show the PCE effect.

II. THE 5*d*-LEVEL ENERGY IN FLUORIDES AND OXIDES

A. Crystal field interaction

The energy $E(Ln^{3+},A)$ to excite a trivalent lanthanide ion Ln^{3+} from its $4f^n$ ground state to the lowest energy $4f^{n-1}5d$ state depends on the type of host crystal A and on the type of Ln^{3+} ion.[20] When Ln^{3+} ions are placed in a crystalline environment, $E(Ln^{3+},A)$ becomes smaller compared to that of free (gaseous) Ln^{3+} ions by an amount $D(Ln^{3+},A)$ called the redshift. It is determined by (i) the crystal field splitting ϵ_{cfs} of the $5d$ configuration and (ii) the centroid shift ϵ_c. The latter is defined as the lowering of the average energy of the five crystal field split $5d$ states relative to the value for the free ion.[22] The situation is illustrated in Fig. 2 for Ce^{3+} where the free ion centroid energy is located at 51 230 cm^{-1}.

Figure 3 shows the influence of the type of host lattice ($LaPO_4$ or LaF_3) and the type of lanthanide ion (Ce^{3+} or Pr^{3+}) on the redshift D and the lowest energy fd-transition E. The lowest $5d$ level of the free ions is chosen as zero point of energy. In the same compound, for example, $LaPO_4$

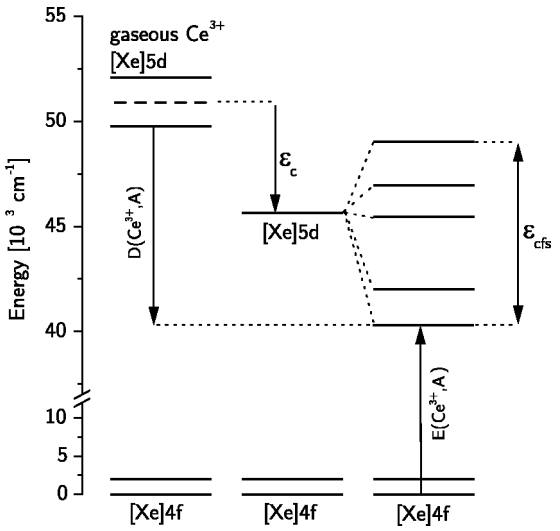

FIG. 2. Schematic representation of the influence of the crystalline environment on the energy of the $[Xe]5d$ electron configuration of Ce^{3+}. The centroid shift ϵ_c, crystal field splitting ϵ_{CFS}, redshift $D(Ce^{3+},A)$, and the lowest energy $4f\rightarrow5d$ transition of Ce^{3+} $E(Ce^{3+},A)$ are indicated.

in Fig. 3, the redshift is the same for Ce^{3+} and Pr^{3+} and in fact for all lanthanides. It implies that the interaction of the $5d$ electron with the crystal field is to first approximation independent on the type of trivalent lanthanide ion. Furthermore Fig. 3 exemplifies that there is a constant energy difference between the $4f\rightarrow5d$ transition energy of Ce^{3+} and that of the $4f^2\rightarrow4f5d$ transition of Pr^{3+}. This difference is independent on the type of host lattice. Therefore, when the energy of the first fd-transition is known for Ce^{3+} in a compound then that of Pr^{3+} when in the same host can be predicted. This predicting tool has been applied successfully by van der Kolk *et al.*[26] to find new host crystals in which the lowest $4f5d$ state of Pr^{3+} is at a higher energy than the $4f^2[^1S_0]$ state.

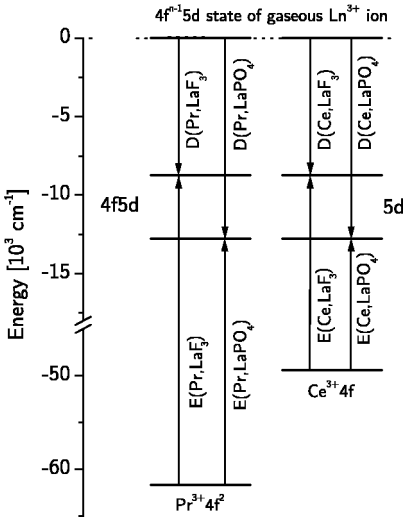

FIG. 3. Schematic representation of the influence of the type of host lattice ($LaPO_4$ or LaF_3) and the type of lanthanide ion (Ce^{3+} or Pr^{3+}) on the redshift D and lowest energy fd-transition E.

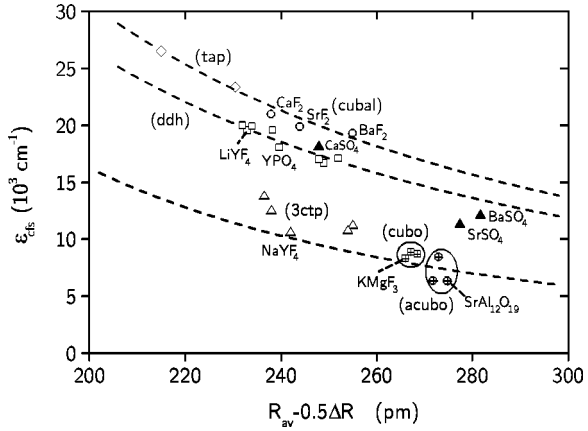

FIG. 4. Total crystal field splitting ϵ_{CFS} of the Ce^{3+} $5d$ configuration against the average Ce^{3+} site size in oxide and fluoride crystals. (tap)= sixfold trigonal antiprism coordination, (cubal) =eightfold cubal coordination, (ddh)=eightfold dodecahedral coordination, (cubo)=twelvefold cuboctahedral coordination, and (acubo)= twelvefold anticuboctahedral coordination. Data obtained from Refs. 22–25.

B. Crystal field splitting

The magnitude of the crystal field splitting ϵ_{CFS} depends on the shape and size of the anion coordination polyhedron around the Ln^{3+} ion. Figure 4 shows results for Ce^{3+} doped materials.[22] ϵ_{CFS} is displayed against the average Ce^{3+} to ligand bond length R in the relaxed oxide and fluoride lattices. The figure demonstrates the effect of site size and polyhedron shape on the crystal field splitting separately. The dashed lines connect fluoride as well as oxide compounds with similar type of polyhedral coordination. For each type of polyhedron, ϵ_{CFS} decreases approximately as R^{-2}. ϵ_{CFS} is large for trigonal antiprism (tap) and cubal coordination, and decreases progressively in going to dodecahedral (ddh), tricapped trigonal prism (3ctp), and cuboctahedral (cubo) and anticuboctahedral (acubo) coordination. The latter three polyhedral coordinations are the most favorable for observing PCE.

C. Centroid energy

Figure 5 demonstrates that the centroid shift ϵ_c tends to increase in going from fluoride compounds to the sulfate, carbonate, phosphate, borate, silicate, and aluminate compounds. The variation of ϵ_c with the type of anion (F^-, Cl^-, Br^-, O^{2-}, S^{2-}) has been discussed often in literature using different models involving the nephelauxetic effect, ligand polarization, or covalency between metal and ligand ions. In each of these models the binding of the ligand charge cloud to cations other than Ce^{3+} is of importance. When it is large, covalency between Ce^{3+} and ligands, ligand polarizability, and nephelauxetic effect are small, and each model predicts a small centroid shift.

In Refs. 22–25 it was found that ϵ_c (cm^{-1}) can be modelled conveniently with

$$\epsilon_c = 1.44\times 10^{17}\frac{N\alpha_{\mathrm{sp}}}{R_{\mathrm{eff}}^6},$$

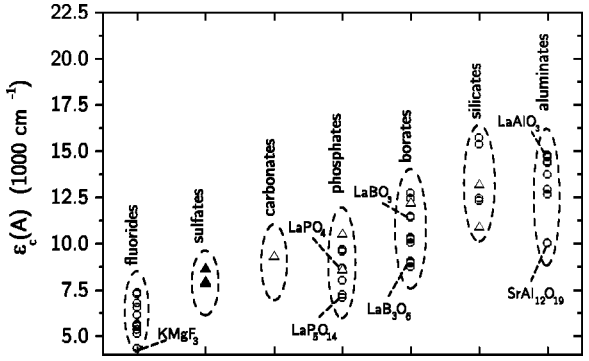

FIG. 5. Centroid shift ϵ_c of the $5d$ configuration of Ce^{3+} in oxide and fluoride crystals. ○, observed values and △, anticipated values from Refs. 22–25. Data for the sulfates are from this work.

$$\frac{1}{R_{\mathrm{eff}}^6} \equiv \frac{1}{N}\sum_{i=1}^{N}\frac{1}{\left(R_i-\frac{1}{2}\Delta R\right)^6}, \tag{1}$$

in which N is the number of ligands in the first coordination sphere each at a distance $R_i-\frac{1}{2}\Delta R$ (pm) from Ce^{3+}. $\frac{1}{2}\Delta R$ has been introduced to account for lattice relaxation around the Ce^{3+} ion. The amount of relaxation is generally not known and as a rough estimation it is assumed that the nearest neighbor fluor ions relax radially inward or outward by half the difference ΔR between the ionic radius of Ce^{3+} and the ionic radius of the cation it substitutes for. α_{sp} (10^{-30} m^3 or $Å^3$), called the spectroscopic polarizability, is a parameter reflecting the average polarizability of the ligands. However, since also covalency and nephelauxetic effect contribute to the centroid shift, their contribution is also represented by α_{sp}. α_{sp} can directly be calculated from the centroid shift and the crystal structure. Data available on the fluorides and oxides reveal clear trends. Whenever small cations with high valency are present they tend to bind the anions and α_{sp} tends to be small. For this reason, ϵ_c increases steadily in the sequence from sulfates to aluminates as in Fig. 5. The ordering is in line with an increasing valency and a decreasing radius of the cation central in the ionic complexes.

The spread in ϵ_c values within one group of compounds is caused by different values for R_i, N, and α_{sp}. α_{sp} was found to decrease with the degree of condensation of ionic complexes in the compound. In the case of phosphates[24] and borates,[25] ϵ_c values tend to decrease when going from orthotype (isolated complexes), to pyrotype (corner sharing complexes), to metatype (rings or chains), and to more condensed phosphates or borates. With increasing degree of condensation, O^{2-} ions are coordinated by more and more small and high charge cations that increase the ligand charge cloud binding. α_{sp} becomes smaller and the centroid shift tends to follows.

For obtaining high energy $5d$ states and the PCE effect of Pr^{3+} to occur, it is clear that the centroid shift should be small. Amongst the oxides this is expected for the sulfate systems: the materials of study in the present work.

III. EXPERIMENTAL TECHNIQUES

A. Material synthesis and structure

Pr^{3+} and Ce^{3+} doped $BaSO_4$, $SrSO_4$, and $CaSO_4$ powder samples, with and without Na^+ codoping for charge compensation, were synthesized by solid state reaction at 850 °C for eight hours in air using $BaSO_4$, $SrSO_4$, $CaSO_4 \times 2H_2O$, $Pr_2(SO_4)_3 \times 8H_2O$, $Ce_2(SO_4)_3$, $Na_2SO_4 \times 10H_2O$ as starting materials. Powder x-ray diffraction analysis (XRD) showed that $BaSO_4$ and $CaSO_4$ were single phased. The XRD spectrum of $SrSO_4$ showed weak lines that could be assigned to the $CaSO_4$ phase next to much stronger lines characteristic for $SrSO_4$.

$BaSO_4$ (barite) and $SrSO_4$ (celestine) are isostructural and have an orthorhombic crystal structure with space group *Pnma* (No. 62). The point symmetry at the Ba and Sr site is C_s, and Ba and Sr are coordinated by 12 O^{2-} ions. Ten O^{2-} ions are at an average distance of 288 and 274 pm,[27,28] while two more O^{2-} ions are found at a larger distance of 332 and 325 pm for $BaSO_4$ and $SrSO_4$, respectively. $CaSO_4$ (anhydrite) has an orthorhombic crystal system with space group *Cmcm* (No. 63). Ca ions are eightfold coordinated by O^2 ions in the form of a dodecahedron at an average distance of 247 pm (Ref. 29) with point symmetry C_{2v}.

B. Spectroscopic techniques

Emission and excitation spectra at 293 K in the 400 to 800 nm wavelength range were performed with a spectrophotometer from Photon Technology International (QuantaMaster model QM-1) with a continuous Xe lamp. Its characteristics were described elsewhere.[30] Between 115 and 650 nm a *f*/4.5, 0.2 m VUV monochromator from Acton Research (model ARC VM-502) was used in combination with a Deuterium lamp (model ARC DS775-100) utilizing MgF_2 coated Al spherical mirrors and grating. Emission was measured either by using a monochromator in combination with a red sensitive Philips XP2254/B PMT, cooled to −20 °C, or an EMI PMT in combination with a MgF_2 collector lens and cutoff and/or interference filters.

Excitation and emission spectra at 10 K were performed at the Deutsche Elektronen Synchrotron (DESY) in Hamburg (Germany) using the SUPERLUMI station of Hasylab. Details of this excitation facility have been described elsewhere.[31] The spectral region of excitation was 50–300 nm with a fixed resolution of 0.3 nm. Luminescence could be detected either in the 150 to 300 nm region utilizing a solar blind PMT or in the 200 to 600 nm region using a cooled Hamamatsu R2059 PMT. The maximal obtainable resolution of both methods was 1 nm. The synchrotron operated in multibunch mode with bunches separated by 200 ns. Emission and excitation spectra were measured within a time window ranging from 2 to 10 ns after the excitation of the sample by the synchrotron pulse. Emission and excitation spectra were also registered without time resolving. We will refer to these measurements as the time resolved and integrated emission or excitation spectra, respectively.

The emission spectra were corrected for wavelength dependent detection efficiency using the best available correction curves. Still, relative emission intensities should be interpreted with care. Excitation spectra were corrected for the wavelength dependent excitation intensity, using sodium salicylate as a reference material.

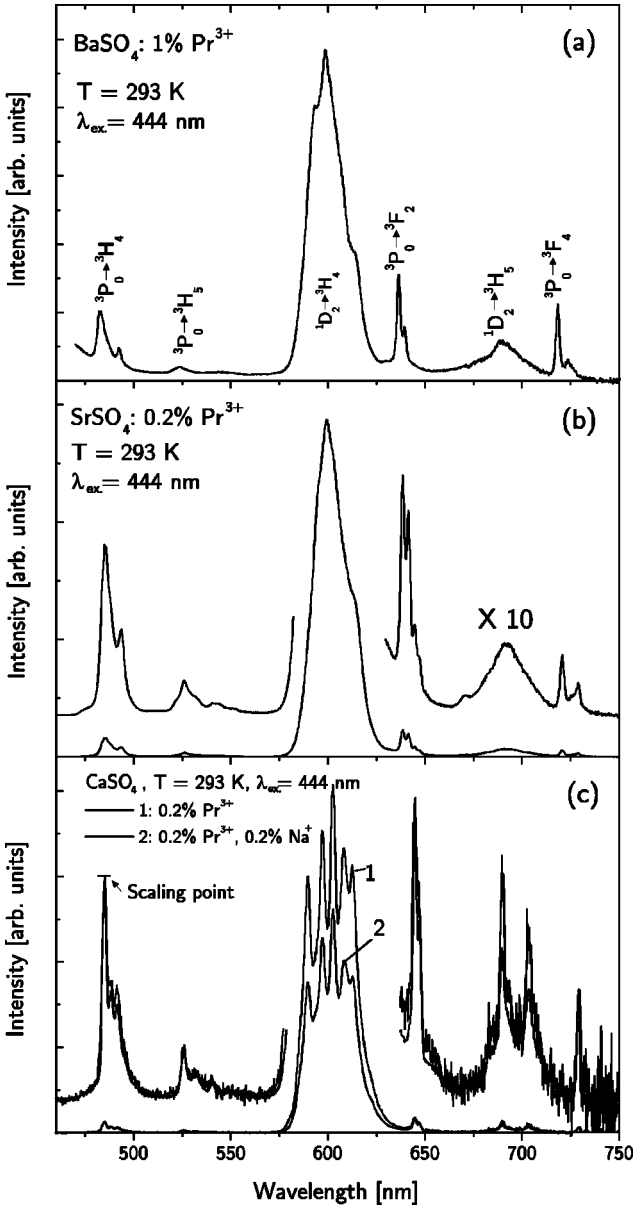

FIG. 6. Luminescence of Pr^{3+} in the visible part of the spectrum at 293 K and $^3P_2$ (444 nm) excitation, when doped in $BaSO_4$ (a), $SrSO_4$ (b), and $CaSO_4$ (c). The $CaSO_4$: 0.2% Pr^{3+} spectrum (1) in Fig. 6(c) was multiplied by 6, so that the $^3P_0 \rightarrow {}^3H_4$ emission intensity equals that of $CaSO_4$: 0.2% Pr^{3+}, 0.2% Na^+.

IV. EXPERIMENTAL RESULTS

A. Emission and excitation properties at 293 K

Figures 6(a)–6(c) show the emission spectra of Pr^{3+} doped $BaSO_4$, $SrSO_4$, and $CaSO_4$ recorded at 293 K under $4f^2[^3H_4] \rightarrow {}^3P_2$ excitation at 444 nm. The spectra are dominated by red $^1D_2 \rightarrow {}^3H_4$ emission around 600 nm. The other much weaker emission lines can be assigned to transitions

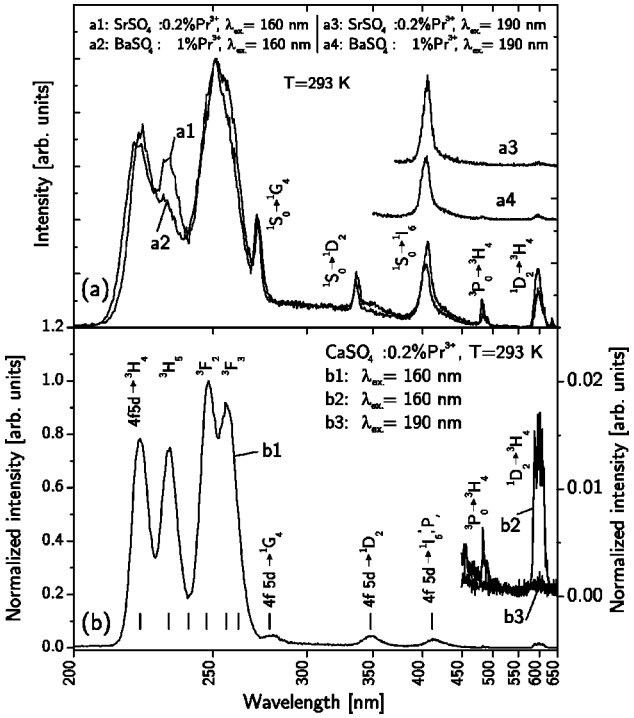

FIG. 7. (a) Emission spectrum of Pr^{3+} recorded at 293 K of $BaSO_4$:1% Pr^{3+} and $SrSO_4$:0.2% Pr^{3+} at 160 nm excitation (spectrum $a2$ and $a1$) and 190 nm excitation (spectrum $a4$ and $a3$). (b) Emission spectrum of Pr^{3+} recorded at 293 K of $CaSO_4$:0.2% Pr^{3+} at 160 nm excitation (spectra $b1$ and $b2$) and 190 nm excitation (spectrum $b3$).

from the $^3P_0$ state to the $^3H_4$, $^3H_5$, $^3F_2$, and $^3F_4$ states. Also $^1D_2 \rightarrow {}^3H_5$ emission is observed around 700 nm.

Codoping $CaSO_4$:0.2% Pr^{3+} with 0.2% Na^+ increased the $^3P_0$ emission intensity by a factor of 6. It is explained by a higher absorption efficiency due to a higher concentration of Pr^{3+} ions in $CaSO_4$ when Na^+ is used as a charge compensating ion. Codoping had only a minor effect for $SrSO_4$ and no effect for $BaSO_4$. It is observed that the $^1D_2$ and the $^3P_0$ emission intensity ratio ($I_{1_{D_2}}/I_{3_{P_0}}$) becomes smaller at a high Pr^{3+} concentration ($BaSO_4$:1% Pr^{3+} and codoped $CaSO_4$:0.2%Pr^{3+}) compared to a lower Pr^{3+} concentration ($SrSO_4$ and $CaSO_4$ with 0.2% Pr^{3+}). This will be discussed in Sec. V A.

Figures 7(a),7(b) show the Pr^{3+} emission recorded at 293 K in $BaSO_4$, $SrSO_4$, and $CaSO_4$ at VUV excitation wavelengths. At 160 nm excitation, $4f5d \rightarrow 4f^2$ as well as $^3P_0$ and $^1D_2$ emission is observed in each sulfate (spectra $a1$-2, $b1$, $b2$). In $BaSO_4$ and $SrSO_4$ also emission from the $^1S_0$ state to the $^1G_4$, $^1D_2$, and $^1I_6$ or ^3P_J states is observed at 271, 336, and 406 nm, respectively. In addition, weak broad band emission between 275 and 375 nm is observed. At 190 nm excitation no $^3P_0$ and $^1D_2$ emission is observed in $CaSO_4$ (spectrum $b3$) and only very weakly in $BaSO_4$ and $SrSO_4$ (spectra $a3$-4). Furthermore, the $4f5d \rightarrow 4f^2$ and $^1S_0$ intensity ratio in $BaSO_4$ and $SrSO_4$ is identical to that observed under 160 nm excitation, while the broad band emission is absent at 190 nm excitation [not shown in Fig. 7(a)].

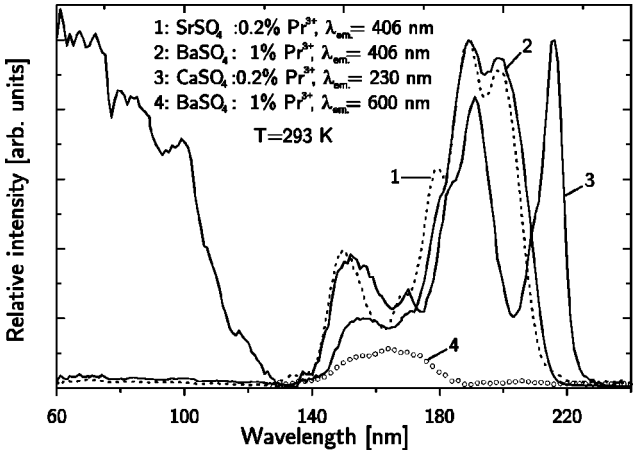

FIG. 8. Excitation spectra, recorded at 293 K, of Pr^{3+} luminescence when doped in $SrSO_4$ (1), $BaSO_4$ (2) monitoring 406 nm emission, $CaSO_4$ monitoring 230 nm emission (3), and in $BaSO_4$ monitoring 600 nm emission (4).

The $CaSO_4$:0.2% Pr^{3+} df emission bands can be assigned to transitions from the lowest $4f5d$-band to the various $4f^2$ states. The most intense emission bands are attributed to transitions to the $^3H_4$, $^3H_5$, $^3F_2$, and $^3F_3$ states while the weaker bands are assigned to transitions to the $^3H_6$, $^3F_4$, $^1G_4$, $^1D_2$, and $^1I_6$ or ^3P_J states. Their positions are indicated in Fig. 7(b) by the vertical lines.

Figure 8 shows excitation spectra at 293 K of Pr^{3+} in $BaSO_4$ and $SrSO_4$, monitoring $^1S_0 \rightarrow {}^1I_6$, ^3P_J emission (spectra 1-2) and $CaSO_4$ monitoring $4f5d \rightarrow 4f^2$ emission (spectrum 3). The excitation spectrum monitoring the $^1D_2 \rightarrow {}^3H_4$ emission (600 nm) in $BaSO_4$ is also included in Fig. 8. Bands between 160 and 220 nm are assigned to excitation to states of the $4f5d$ configuration of Pr^{3+}. The lowest energy $4f5d$ level in $BaSO_4$ and $SrSO_4$ is found at 199 nm while that in $CaSO_4$ is found at 216 nm. The bands around 150 nm in $CaSO_4$ and $SrSO_4$ and 155 nm in $BaSO_4$ are assigned to the host lattice excitation and are further discussed below. When the $^1D_2 \rightarrow {}^3H_4$ emission is monitored in $BaSO_4$, the host lattice excitation bands between 135 and 180 nm are the only ones observed. Excitation below 125 nm (<10 eV) results in $4f5d \rightarrow 4f^2$ emission in the case of $CaSO_4$ while no emission is observed in $BaSO_4$ and $SrSO_4$.

The VUV absorption and emission properties of undoped sulfates were investigated for K_2SO_4 (Refs. 32–36) and $CaSO_4$ (Refs. 35,36) by means of diffuse reflection and luminescence excitation spectroscopy. Although optical properties appear different from one sulfate to the other and bands cannot always be identified uniquely, sulfates seem to have two distinct types of host lattice excitation. One excitation region, at relatively low energy between 6 and 10 eV, is attributed to excitation of the SO_4^{2-} complex, and a region at higher energy (>9 eV) is assigned to valence band to conduction band transitions. We therefore assign the bands observed between 140 and 180 nm in Fig. 8 to excitations involving the SO_4^{2-} complex. The excitation region below 125 nm (≈ 10 eV) observed in the spectrum of $CaSO_4$ is assigned to valence band to conduction band excitation.

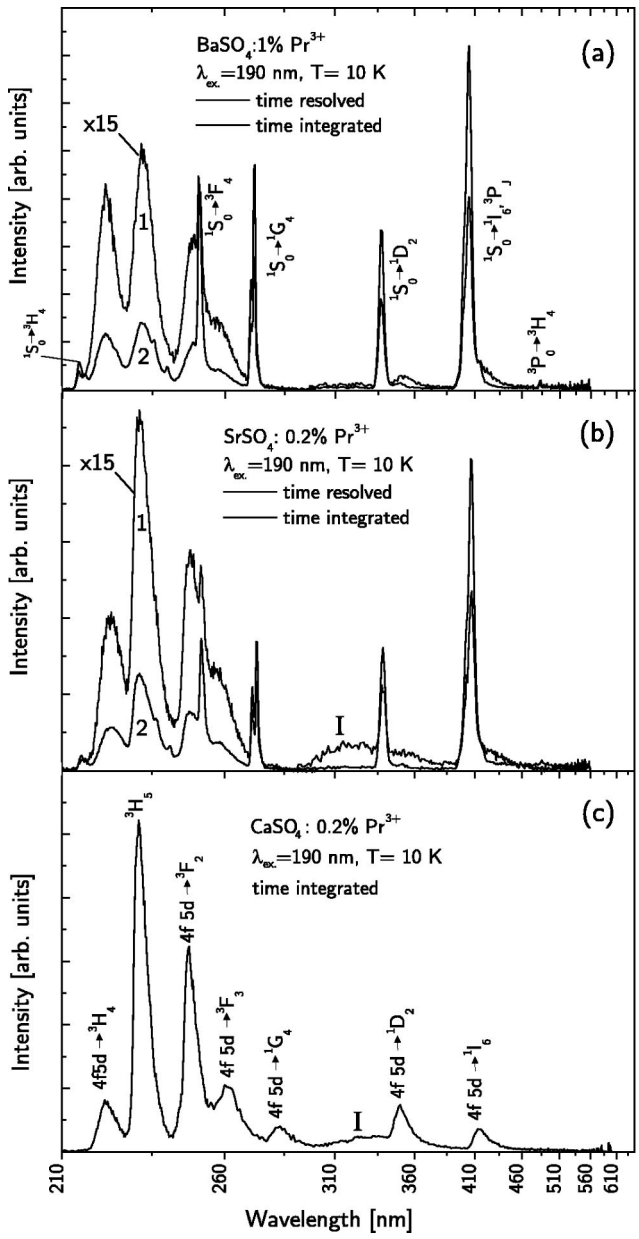

FIG. 9. Time integrated emission spectra and time resolved emission spectra recorded at 10 K under 190 nm excitation of $BaSO_4$:1% Pr^{3+} (a), $SrSO_4$:0.2% Pr^{3+} (b), and $CaSO_4$:0.2% Pr^{3+} (c). The time resolved emission spectra were obtained by collecting light between 2 and 10 ns after the synchrotron excitation pulses.

B. Emission and excitation properties at 10 K

In Figs. 9(a), 9(b) the time resolved and time integrated emission spectra of $BaSO_4$ and $SrSO_4$ recorded at 10 K and 190 nm excitation are compared. When light is collected between 2 and 10 ns after pulsed synchrotron excitation, mainly fast $4f5d \rightarrow 4f^2$ emission is observed (spectra 1). Emission band assignments are identical to that of $CaSO_4:Pr^{3+}$ at 293 K, see Fig. 7(b). $^1S_0 \rightarrow {}^3F_4$, $^1G_4$, $^1D_2$, and $^1I_6$ or ^3P_J transitions are observed at 251, 272, 337, and 406 nm. In the time integrated spectra (spectra 2), also the $^1S_0 \rightarrow {}^3H_4$, $^3H_6$, and $^3F_2$ emission lines are observed at 214, 236, and 240 nm. The $4f5d \rightarrow 4f^2$ emission is considerably less intense relative to the $^1S_0$ emission at 10 K [see Figs. 9(a), 9(b)] than at 293 K [see Fig. 7(a)]. The integrated emission spectrum of $CaSO_4$ recorded at 10 K is shown in Fig. 9(c). The emission bandwidths have decreased from about 1400 cm^{-1} at 293 K to 1000 cm^{-1}, and the relative emission intensities of the different $d \rightarrow f$ bands have changed compared to the situation at 293 K. The broad emission observed in $CaSO_4$ and $SrSO_4$ around 340 nm (designated by *I*) was also observed by Lakshmanan *et al.* in Ln^{3+} doped $CaSO_4$ in thermally stimulated and cathode ray excited luminescence spectra.[37]

Figures 10(a)–10(c) show the 10 K excitation spectra of $BaSO_4:Pr^{3+}$ (a) and $SrSO_4:Pr^{3+}$ (b) monitoring $^1S_0 \rightarrow {}^1I_6$ emission (406 nm), and of $CaSO_4:Pr^{3+}$ (c) monitoring $4f5d \rightarrow 4f^2$ emission (230 nm). The spectra show more structure than the spectra recorded at 293 K (see Fig. 8) due to the smaller bandwidths. The inset of Fig. 10(a) shows a weak and a more stronger $^3H_4 \rightarrow {}^1S_0$ transition at 46 730 and 46 880 cm^{-1}. This implies the presence of at least two different Pr^{3+} sites in $BaSO_4$ that have the $^1S_0$ state isolated from the $4f5d$ states. In $SrSO_4$ the $^1S_0 \rightarrow {}^3H_4$ transition is observed at 46570 cm^{-1}. It has a 200 times lower intensity than the $f \rightarrow d$ transitions due to the parity forbidden nature of the $f \rightarrow f$ transition.

Figures 10(a)–10(c) also show the 293 K excitation spectra monitoring the Ce^{3+} $d \rightarrow f$ emission in the same compounds. Since, if put in the same compound, the first fd transition of Pr^{3+} always occurs at about 12 200 ± 600 cm^{-1} higher energy than that of Ce^{3+},[20] we have shifted the original Ce^{3+} excitation spectra towards higher energy. The energy shift was chosen such that the first fd transition coincide for both lanthanides. The applied shifts, all within $12\,200 \pm 600$ cm^{-1}, are indicated in the figures.

The energy of the five $5d$ crystal field states of Ce^{3+}, their average energy E_c, the centroid shift ϵ_c, and the total crystal field splitting ϵ_{CFS} are listed in Table I. In the same table the energies of the first $4f^2 \rightarrow 4f5d$ transition in Pr^{3+} and the $4f^7 \rightarrow 4f^6[^7F_0]5d$ transition in Eu^{2+} from Ref. 38 are included.

The lowest energy $4f \rightarrow 5d$ bands of Ce^{3+} in $BaSO_4$ and $SrSO_4$ reveal a shoulder on the low energy site. This has been studied in more detail by Vink *et al.*[39] and is not related to the Ce^{3+} center of Table I. Also the excitation peak in $BaSO_4:Ce^{3+}$ around 50 000 cm^{-1} is of different origin.

The excitation bands at 155 and 160 nm in the Pr^{3+} doped sulfates that were related to excitation of the sulfate group, are also observed in the Ce^{3+} excitation spectra at the same wavelengths. Because of the 12 374 cm^{-1} shift applied to the spectrum of $CaSO_4:Ce^{3+}$ shown in Fig. 10(c), it appears at 125 nm. The actual maximum is found at 147 nm. The same bands are also observed in the Pr^{3+} excitation spectra, which demonstrates that they are not related to the $4f5d$ configuration of Pr^{3+}.

In Fig. 11 the 10 K excitation spectra of $BaSO_4:Pr^{3+}$, monitoring the $4f5d \rightarrow 4f^2$ emission at 232 nm (1) and $^1S_0 \rightarrow {}^1I_6$ or ^3P_J emission at 406 nm (2), are compared. Below 190 nm the two spectra are of identical shape. How-

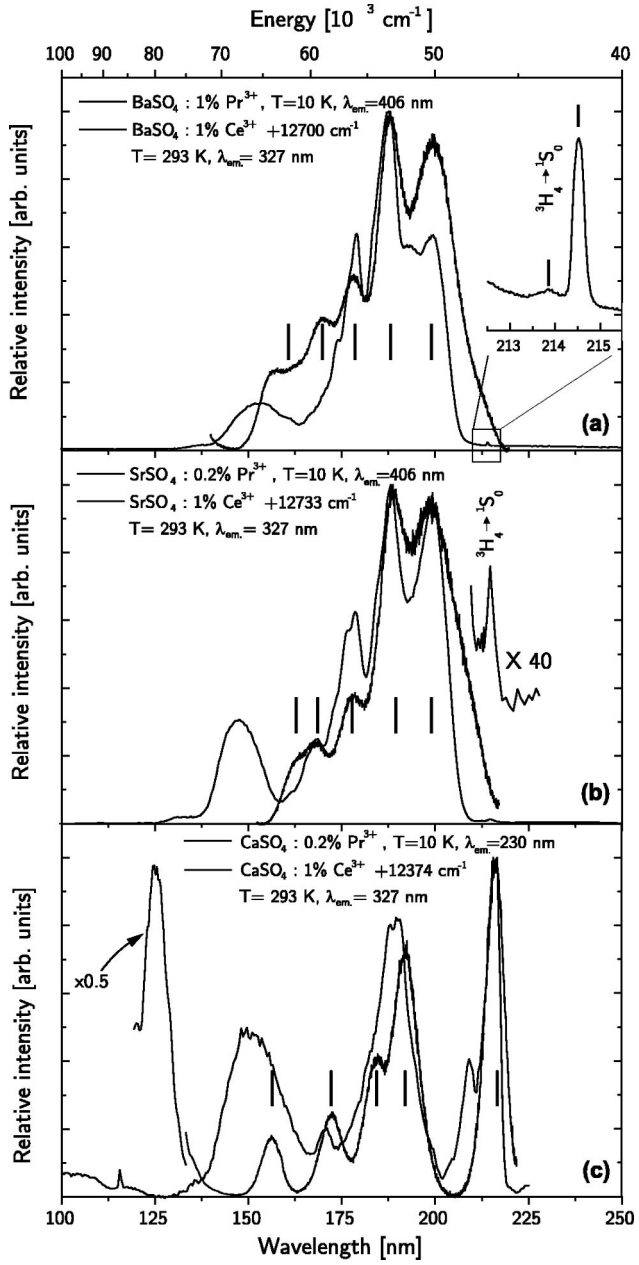

FIG. 10. A comparison between the VUV excitation spectra of Ce^{3+} and Pr^{3+} doped in $BaSO_4$ (a), $SrSO_4$ (b), and $CaSO_4$ (c). The Ce^{3+} spectra were shifted to higher energy until the lowest $5d$ state coincides with that of Pr^{3+}. See text and figure for further detail.

ever, above 190 nm they are markedly different. The 203 nm excitation band is observed with a much higher intensity when $5d \rightarrow 4f$ emission is monitored. This observation may be indicative for the presence of two different Pr^{3+} sites in $BaSO_4$.

Figure 12 shows the 10 K excitation spectrum of $BaSO_4$:1% Pr^{3+} monitoring 360 nm emission and the emission spectrum at 160 nm excitation. The excitation band at 160 nm was also observed in all other excitation spectra presented before. The emission spectrum observed at 160 nm excitation consists of $^1S_0$ emission and $^3P_0$ emission lines, but also a broad emission band peaking at 310 nm is observed. Because of the large width (100 nm FWHM), the large stokes shift, and the energy (32×10^3 cm^{-1}) of this emission, and because the emission can only be observed under host lattice excitation, it is assigned to self-trapped-exciton (STE) emission. The $4f5d \rightarrow 4f^2$ emission intensity is small compared to the $^1S_0$ emission intensity. This is partly due to the low detection efficiency of the equipment at wavelengths shorter than 250 nm, but still we have to conclude that at 10 K $4f5d \rightarrow 4f^2$ emission is weak compared to $^1S_0$ emission, see Figs. 7(a) and 9(a),9(b). Compared to the situation at 293 K in Fig. 7(a), the STE emission intensity at 10 K is much more intense relative to $^1S_0$ emission intensity. In this respect it is noted that STE emission is often quenched at 293 K.

TABLE I. $4f \rightarrow 5d$ transition energies E_{fd}, centroid energy E_c, centroid shift ϵ_c, and crystal field splitting ϵ_{CFS} of Ce^{3+} in $BaSO_4$, $SrSO_4$, and $CaSO_4$. $E(Pr^{3+})$ and $E(Eu^{2+})$ are the lowest energy $4f \rightarrow 5d$ transition of Pr^{3+} and Eu^{2+}. All energies are in cm^{-1}.

	$BaSO_4$	$SrSO_4$	$CaSO_4$
E_{fd}	37 400	37 500	33 800
	40 500	40 300	40 000
	43 300	43 400	41 900
	46 200	46 800	45 400
	49 500	48 800	51 900
$E_c(Ce^{3+})$	43 400	43 300	42 600
$\epsilon_c(Ce^{3+})$	7840	7930	8630
$\epsilon_{\mathrm{CFS}}(Ce^{3+}$	12 100	11 300	18 100
$E(Pr^{3+})$	50 500	50 200	46 200
$E(Eu^{2+})$	29 000	29 000	26 400

The nature of the excitation bands between 185 and 255 nm is unclear, but may be related to excitation of defects such as SO_4^- or SO_3^- formed during synthesis or induced by VUV radiation. Similar absorption bands of various defect emissions in $CaSO_4$, reviewed recently by Lakshmanan *et al.*,[40] are found between 200 and 400 nm. Excitation at 230 nm results in broad emission between 300 and 500 nm.

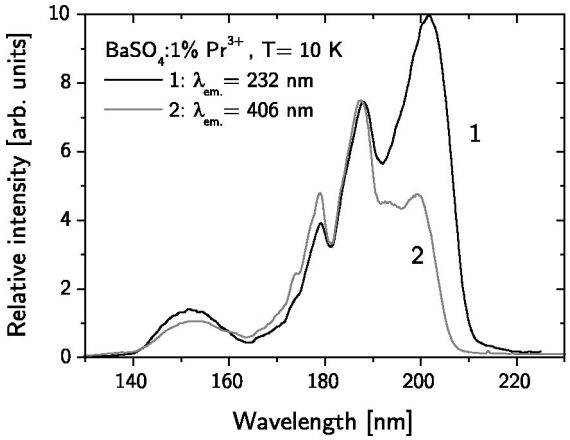

FIG. 11. Excitation spectra of Pr^{3+} in $BaSO_4$ recorded at 10 K monitoring $4f5d \rightarrow 4f^2$ emission at 232 nm (spectrum 1) and $^1S_0 \rightarrow {}^1I_6$ or ^3P_J emission at 406 nm (spectrum 2).

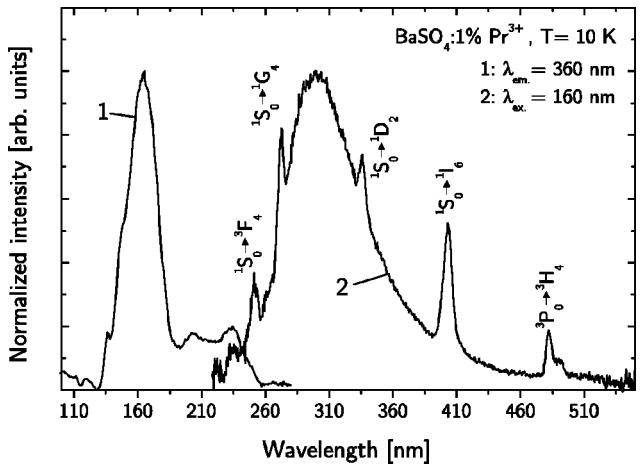

FIG. 12. Emission spectrum at 160 nm excitation (spectrum 2) and excitation spectrum monitoring 360 nm STE emission (spectrum 1) of Pr^{3+} in $BaSO_4$ recorded at 10 K.

V. DISCUSSION

A. Radiative and nonradiative $4f^2$ transitions

The $^1D_2 \rightarrow {}^3H_4$ emission that is observed under $^3P_2$ excitation in Fig. 6 is attributed to a high $^3P_0 \rightarrow {}^1D_2$ multiphonon relaxation rate Γ_{nr}. With the relatively high maximum phonon energies $\hbar\omega_{\max} \approx 1100$ cm^{-1},[41] corresponding to the stretching vibrations of the S-O bond in the SO_4^{2-} complex, and a small energy gap of about 4000 cm^{-1} between the $^3P_0$ and $^1D_2$ states, multiphonon relaxation involves the emission of minimal four phonons. The energy gap between the $^1D_2$ and $^1G_4$ states is about 6300 cm^{-1} and according to the energy gap law in revised form of van Dijk and Schuurmans,[42] $\Gamma_{nr}(T=0\ \mathrm{K}) \propto \exp[-\alpha(\Delta E - 2\hbar\omega_{\max})]$, describing the multiphonon relaxation rate Γ_{nr} with an accuracy of about two orders of magnitude, the $^1D_2 \rightarrow {}^1G_4$ nonradiative rates can be estimated to be 10^{-4} times smaller. We used $\alpha = 4.5(\pm 1.0) \times 10^{-3}\mathrm{cm}^{-1}$ from Ref. 44. It is therefore not surprising that the emission properties of Pr^{3+} in these sulphates are dominated by the red $^1D_2 \rightarrow {}^3H_4$ transition.

The cascade emission process of Pr^{3+} provides a unique opportunity to determine the internal quantum efficiency of emitting levels that are populated by the emission from the $^1S_0$ state. Spectrum *a*4 of Fig. 7(a) shows that for $BaSO_4$ the $^1D_2$ emission at 600 nm has intensity about 1% of that of the $^1S_0 \rightarrow {}^1I_6, {}^3P_J$ emission at 406 nm. This implies that the QE of the $^1D_2$ emission can not be higher than about 1%. From Fig. 6(a) and the discussion in the beginning of this section, the QE of the $^3P_0$ emission is found to be 0.1%. Similar arguments for $SrSO_4$ yield even lower QE's.

The measured QE may be compared with the QE calculated using the expression QE=100% $\times \Gamma_r/(\Gamma_{nr}+\Gamma_r)$, where Γ_r is the total radiative transition rate. Γ_{nr} values calculated using the energy gap law for the $^3P_0$ and $^1D_2$ states are 10^3–10^4 s^{-1} and 10^{-1} s^{-1}, respectively. Typical radiative rates at low Pr^{3+} concentration of the $^3P_0$ and $^1D_2$ emission are 10^4 and 10^3 s^{-1}, respectively.[43,44] The calculated QE's are thus orders of magnitude too low compared to the measured values. This may reflect the limitations of the energy gap law, but may also indicate that other quenching processes like energy migration to quenching sites or cross relaxation play a role.

The importance of the latter two processes depend on the Pr^{3+} concentration and have been studied in detail in oxides and fluorides. Generally, it is found that quenching of the $^1D_2$ emission occurs at lower concentration than quenching of the $^3P_0$ emission.[43,45–47] This may explain the higher $^3P_0$ emission intensity relative to the $^1D_2$ intensity in $BaSO_4$:1% Pr^{3+} and $CaSO_4$:0.2% Pr^{3+},0.2% Na^+ compared to the intensity in $CaSO_4$:0.2% Pr^{3+} and $SrSO_4$:0.2% Pr^{3+} with a lower Pr^{3+} concentration.

B. $4f^2[^1S_0] \rightarrow 4f^2$ and $4f5d \rightarrow 4f^2$ emission

The simultaneous observation of $4f^2[^1S_0] \rightarrow 4f^2$ line emission and $4f5d \rightarrow 4f^2$ broad band emission in $BaSO_4$ and $SrSO_4$, see Figs. 7 and 9, suggests the presence of two different Pr^{3+} sites. One site has then the lowest $5d$ level above the $^1S_0$ level, and the other site has the $5d$ level below the $^1S_0$ level. In the case of $BaSO_4$:Pr^{3+}, Fig. 10 also shows evidence of two sites because two different $^3H_4 \rightarrow {}^1S_0$ excitation lines are observed. Both $SrSO_4$ and $BaSO_4$ have, however, only one crystallographic site available for Pr^{3+}. The possible two different sites may be related to the presence or absence of charge compensating defects.

An alternative model to explain the $5d$-emission bands involves thermal excitation from the $^1S_0$ state to the lowest energy $4f5d$ state. In this case both $^1S_0$ and df-luminescence may originate from the same Pr^{3+} center. Indeed, the ratio between the $d \rightarrow f$ emission intensity and the $^1S_0$ emission intensity, strongly depends on temperature. Figure 7 shows that at 293 K df emission is much more intense than $^1S_0$ emission. As can be seen in Fig. 9, the situation is reversed at 10 K. This behavior closely resembles that observed for the luminescence of Eu^{2+} in $BaSO_4$ and $SrSO_4$.[38] It is also observed in the fluorides $KMgF_3$ (Ref. 48) and $LiBaF_3$,[49] and in the borate SrB_4O_7.[50] In these materials, the $4f^6 5d$ state of Eu^{2+} is located just above the opposite parity $4f^7[^6P_{7/2}]$ state. Both $4f^7[^6P_{7/2}] \rightarrow {}^8S_{7/2}$ line and $4f^6 5d \rightarrow 4f^7$ broad band emission are observed, originating from the same Eu^{2+} center. It is commonly accepted that the $5d$ state is reached by thermal excitation from the $^6P_{7/2}$ state.

Based on the similarity with Eu^{2+} luminescence, we may conclude that the df emission and $^1S_0$ emission of Pr^{3+} in $BaSO_4$ and $SrSO_4$ stem from one type of Pr^{3+} center. What still remains to be explained are the differences between the 10 K excitation spectra shown in Fig. 11 at wavelengths between 190 and 210 nm. One may speculate that after excitation of the $4f5d$ configuration, relaxation to the $^1S_0$ state or to the lowest energy $4f5d$ states takes place, with a certain branching ratio that depends on the wavelength of excitation. Relaxation to the $^1S_0$ state seems then to have higher probability at excitation wavelengths above 200 nm. The transitions starting from the $^1S_0$ state will show a longer decay time compared to parity allowed df-emission transitions. The model involving thermal excitation from the $^1S_0$ state to the $5d$ states, predicts changes in the effective life-

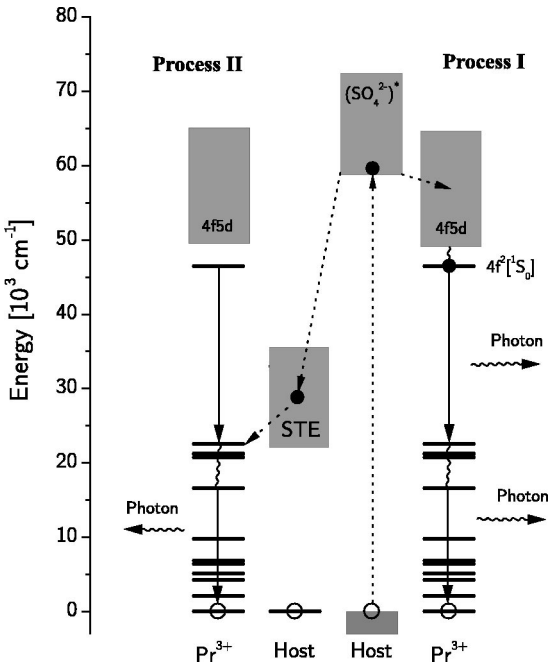

FIG. 13. Schematic representation of direct electron-hole pair recombination involving the $4f5d$ states leading to Pr^{3+} $^1S_0$ excitation (process I) and Pr^{3+} $^3P_0$ excitation via an intermediate STE state (process II).

times of the $^1S_0$ state and $5d$ state. It is therefore of interest to measure these lifetimes as function of temperature to test its validity.

C. Host lattice to Pr^{3+} energy transfer

In this work we distinguish two mechanisms of energy transfer from host to Pr^{3+} center. Electron and hole pairs created upon host lattice excitation can be trapped by Pr^{3+} ions leading to an immediate excitation (process I). They may also form of a self-trapped-exciton (STE) state that can transfer its energy to a Pr ion (process II). Similar types of mechanisms are thought to occur in Ce^{3+} doped scintillator materials upon excitation with ionizing radiation.[30,51,52] The situation is illustrated in Fig. 13.

Under 190 nm excitation, Pr^{3+} is excited directly into one of its $4f5d$ states resulting in $4f5d \rightarrow 4f^2$ emission in the case of Ca, Sr, or $BaSO_4$, and $^1S_0$ emission in the case of $BaSO_4$ and $SrSO_4$ (see Figs. 7 and 8). Due to the PCE process, although with very low QE, $^3P_0$ and $^1D_2$ emission is observed in Fig. 7(a) spectrum 3 and 4.

At 160 nm excitation, emission from the $^3P_0$ and $^1D_2$ states is much more intense than at 190 nm. This holds for $BaSO_4$ and $SrSO_4$ [Fig. 7(a), spectrum 1-2] as well as for $CaSO_4$ [Fig. 7(b), spectrum 2]. The $^3P_0$ and $^1D_2$ emission at 160 nm excitation cannot be the result of the PCE process since this would imply QE's close to unity for the $^1D_2$ state, which is in contradiction to what was concluded at 190 nm excitation. Instead, it must be concluded that part of the host lattice excitation energy is transferred to the $^3P_0$ and $^1D_2$ state, not involving the $4f5d$ or $^1S_0$ states of Pr^{3+}. This is confirmed by the excitation spectrum (Fig. 8, spectrum 4) of the $^1D_2$ emission at 600 nm in which only the host lattice excitation bands appear between 140–180 nm.

The following model is proposed. At 160 nm excitation, SO_4^{2-} complexes are excited which transfer their energy to the $4f5d$ states of Pr^{3+} ions via a fast process. This is process I in Fig. 13. It results in identical emission features as observed under 190 nm excitation. Excited SO_4^{2-} complexes may also create a self-trapped-exciton-like state. The STE can decay radiatively yielding the broad emission observed in Fig. 12, or it can transfer its energy to the ^3P_J and $^1I_6$ states of a Pr^{3+} ion, resulting mainly in $^1D_2$ emission. This is process II in Fig. 13. No $4f5d \rightarrow 4f^2$ or $^1S_0$ emission will result in this process.

The existence of STE's is evidenced by the broad emission observed at 10 K in $BaSO_4$ at about 310 nm, see Fig. 12. This emission can only be excited in a band centered at 160 nm that was assigned to the excitation of SO_4^{2-} complexes. Observation of the same band when monitoring the $^1D_2 \rightarrow {}^3H_4$ nm emission evidences the excitation transfer via the STE's. The small spectral overlap between the STE emission and the ground state to ^3P_J and $^1I_6$ absorption lines results in rather poor energy transfer efficiency. Since also quantum splitting does not take place, the STE mediated energy transfer is a highly unwanted process if one considers application as phosphors in Plasma Display Panels or Xe filled lighting tubes.

D. Crystal field interaction of the $4f^{n-1}5d^1$ states of Ce^{3+}, Pr^{3+}, and Eu^{2+}

Data on all five $5d$-level energies ϵ_{CFS} and ϵ_c of Ce^{3+} in sulfates were not known before this work. The values for the centroid shift in $CaSO_4$, $SrSO_4$, and $BaSO_4$ found in this work and compiled in Table I were also used in Fig. 5. They are smaller than those in the orthophosphate $LaPO_4$ (8660 cm^{-1}) and orthoborate $LaBO_3$ (11450 cm^{-1}). This is in line with the stronger binding in the sulfate complex as compared to the phosphate and borate complexes.

The crystal field splitting in $BaSO_4$ appears slightly larger than that in the isostructural $SrSO_4$. Based on the larger site size available for Pr^{3+} in $BaSO_4$ compared to that in $SrSO_4$, however, a smaller crystal field splitting is expected. Possibly relaxation around Pr^{3+} on the large Ba^{2+} site is responsible for this. The crystal field splitting in $CaSO_4$ (18×10^3 cm^{-1}) is considerably larger than that in $BaSO_4$ and $SrSO_4$ (12×10^3 cm^{-1}). The coordination around Ca^{2+} is eightfold in the form of a dodecahedron. Crystal field splitting falls perfectly on the curve in Fig. 4 pertaining to compounds with dodecahedral coordination like YPO_4 and $LiYF_4$. The large crystal field splitting in $CaSO_4$ is the mean reason for absence of PCE.

The energy of the lowest $5d$ state of Ce^{3+}, Pr^{3+}, and Eu^{2+} behaves similarly with changing crystalline environment. This is demonstrated in Fig. 14. The dashed lines connect the lowest energy $5d$ states of Ce^{3+}, Pr^{3+}, and Eu^{2+} in $BaSO_4$, $SrSO_4$, and $CaSO_4$. For Ce^{3+} all five $5d$ levels are shown. For Pr^{3+} and Eu^{2+} the $^1S_0$ and $^6P_{7/2}$ levels are shown. The energy of the lowest $5d$ state of Pr^{3+} $E(Pr^{3+})$ decreases considerably when going from $SrSO_4$ to $CaSO_4$,

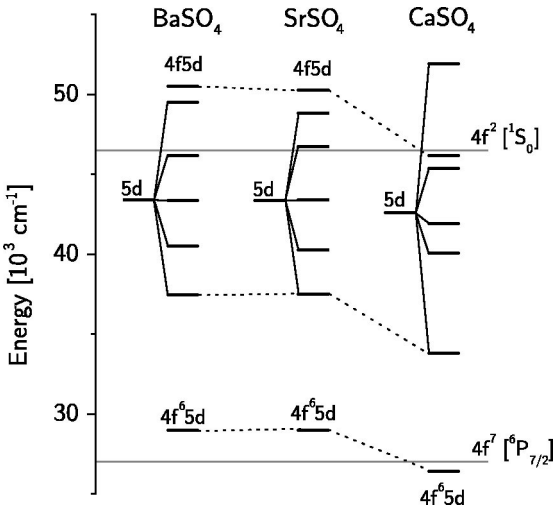

FIG. 14. Schematic representation of the crystal field splitting of the $5d$ configuration of Ce^{3+}, the lowest energy $4f5d$ states of Pr^{3+} and the lowest energy $4f^6 5d$ states of Eu^{2+} in $BaSO_4$, $SrSO_4$, and $CaSO_4$. The lowest energy $5d$ states of Ce^{3+}, Pr^{3+}, and Eu^{2+} are connected by dashed lines. The energy of the $^1S_0$ state of Pr^{3+} and the $^6P_{7/2}$ state of Eu^{2+} are indicated by horizontal line.

and the energy falls just below the $^1S_0$ state. The change in $E(Ce^{3+})$ and $E(Pr^{3+})$ is of equal magnitude which is in line with the constant energy difference always observed between $E(Ce^{3+},A)$ and $E(Pr^{3+},A)$ in the same host A, see Ref. 20 and Sec. II A.

Figure 14 also shows that the decrease in $E(Ce^{3+})$ and $E(Pr^{3+})$ from $SrSO_4$ to $CaSO_4$ is about twice as large as for Eu^{2+}. This was also noticed by van der Kolk *et al.*,[26] where $E(Ce^{3+},A)$, $E(Pr^{3+},A)$, and $E(Eu^{2+},A)$ values in many different host lattices were compared. Apparently the $5d$-level energies in Eu^{2+} are less influenced by the crystal field than those of the trivalent lanthanides.

Figure 10 shows that the excitation spectra of Pr^{3+} in $BaSO_4$, $SrSO_4$, and $CaSO_4$ closely resemble those of Ce^{3+} in the same compounds. Despite the more complicated electron configuration in Pr^{3+} ($4f5d$) compared to Ce^{3+} ($5d$), the shape of the excitation spectra of Pr^{3+} is apparently still dominated by the crystal field interaction with the $5d$ electron. A more thorough discussion on a theoretical and experimental comparison between Ce^{3+} and Pr^{3+} excitation spectra was recently presented by Laroche *et al.*[53] and Reid *et al.*[54] for the case of $LiYF_4$. In these works the additional structural features in the Pr^{3+} excitation spectra were interpreted by a Coulomb interaction between the $5d$ electron and the $4f$ electron, the spin-orbit interaction of the $4f$ electron, and its interaction with the crystal field.

VI. PREDICTING PCE IN OTHER INORGANIC COMPOUNDS

The requirements for photon cascade emission by Pr^{3+} in compounds can be formulated in terms of centroid shift ϵ_c and crystal field splitting ϵ_{CFS}, i.e., in terms of the redshift $D(Pr,A)$. The lowest energy $4f5d$ state of Pr^{3+} must be above the $^1S_0$ state which is found at about 47 000 cm^{-1}. The free Pr^{3+} ion value being 61 200 cm^{-1}, implies that the red shift must be smaller than 14 000 cm^{-1} (see Fig. 3). Taking into account a possible Stokes shift $\Delta S \approx 2900$ cm^{-1}, which is a typical Stokes shift value,[21] the limiting redshift value becomes $\approx 12\,500$ cm^{-1}. Note that the lattice relaxation reduces the energy difference between the $5d$ and $^1S_0$ by only $\Delta S/2$. The other part stems from relaxation occurring after the transition to the ground state of Pr^{3+} has taken place.

One may now apply the redshift and Stokes shift values collected in Ref. 21 for Ce^{3+} doped compounds as a starting point to find compounds that support PCE. Such approach was taken in Ref. 26. One may also apply the trends[22–25] observed in the crystal field splitting and centroid shift of the $5d$ configuration of Ce^{3+} to select compounds for which redshift values are not yet available. Below we will follow this approach.

In *fluorides* the largest contribution to the redshift stems from the crystal field splitting. Figure 5 shows that the centroid shift varies weakly between 4500 and 7500 cm^{-1}. Therefore, fluorides with sufficiently small ϵ_{CFS} support PCE. This is often the case when the coordination number N is larger than eightfold as in YF_3, LaF_3, and $NaYF_3$. Especially when the coordination is in the form of a tri-capped trigonal prism ($NaYF_3$) or a cuboctahedron ($KMgF_3$) crystal field splitting is small, see Fig. 4.

Eightfold coordination generally has larger ϵ_{CFS}, see Fig. 4, and for example PCE is not expected in the cubic fluorites (BaF_2, SrF_2, and CaF_2) and in most compounds with dodecahedral coordination such as $LiYF_4$. Only when the centroid shift is small, PCE may still occur. Small centroid shift is promoted when small and highly charged cations such as Al^{3+}, Zr^{4+}, B^{3+}, Be^{2+}, or Si^{4+} are present in the compound. We recently studied $LaZrF_7:Pr^{3+}$ which indeed supports PCE.[55]

The smallest centroid shift values amongst the ''complex'' oxides are expected for the *sulfates*. Depending on the crystal field splitting this can result in PCE as is indeed observed in this work for $BaSO_4$ and $SrSO_4$. Also in other sulfates, i.e., $La_2(SO_4)_3$, $LiLa(SO_4)_2$, $NaLa(SO_4)_2$, and $BaMg(SO_4)_2$, we observed PCE.[56] It seems that most sulfates with Pr^{3+} on large metal ion sites like Ba^{2+}, Sr^{2+}, La^{3+}, and possibly also Y^{3+}, support PCE.

Carbonates are positioned between the sulfates and phosphates in Fig. 5. Although almost no spectroscopic data is available on lanthanide doped carbonates, relatively small values for the centroid shift are anticipated. Provided that the crystal field splitting is small, PCE seems possible. $SrCO_3$ and $La_2(CO_3)_3$ are interesting test cases in this respect.

Of all *phosphates*, sofar the smallest redshift (12 800 cm^{-1}) is observed for $LaPO_4$. Nevertheless, when doped with Pr^{3+}, $4f5d \rightarrow 4f^2$ emission is observed. The absence of PCE in $LaPO_4$ is related to the large Stokes shift of 5160 cm^{-1}.[21] All other phosphates studied sofar have at least 2000 cm^{-1} larger redshift and do not support PCE. Still, the pyrophosphate $Ba_2(P_2O_7)$ and the condensed phosphate $Ba(PO_3)_2$ are worthwhile studying.

Within the *borates*, the smallest values for the centroid

shift are observed for the condensed borates. $LaMgB_5O_{10}$ and LaB_3O_6 support PCE, see Refs. 17,18. Their ϵ_c and ϵ_{CFS} values are practically the same as in $LaPO_4$ but the Stokes shift for Ce^{3+} is smaller, i.e., $\Delta S \approx 3700$ cm^{-1}.[21] Also SrB_4O_7 shows PCE when doped with Pr^{3+} as was recently demonstrated by van der Kolk *et al.*[57] SrB_6O_{10} is another possible candidate. PCE will be rather unlikely in the orthoborates. Only in the condensed borates in which Pr^{3+} replaces large cations such as La^{3+}, Sr^{2+}, or Ba^{2+} PCE may take place.

According to Fig. 5 the centroid shift in the *silicates* is even larger than in the borates. Silicates doped with Ce^{3+} studied so far have redshifts larger than 17 000 cm^{-1}. One exception is the small redshift of 14 250 cm^{-1} for Ce^{3+} on the La^{3+} site on the Wyckoff $4f$ position in the apatite structure of $La_{9.33}(SiO_4)_6O_2$. The tricapped trigonal prism type of coordination results in relatively small crystal field splitting, but still redshift is too large for PCE.

The $^6P_{7/2} \rightarrow {}^8S_{7/2}$ line emission of Eu^{2+}, observed in the pyrosilicate $SrBe_2Si_2O_7$ by Verstegen *et al.*[58] suggests that the redshift must be small in this compound and probably PCE will take place. Apparently, the presence of small Be^{2+} cations, the condensation of the silicate complexes into pyrogroups, and the large Sr^{2+} site yields small centroid shift and small crystal field splitting. In this respect $Ba(Si_4O_9)$ may be interesting candidate material.

The redshift in the *aluminates* shows a very wide range extending from 11 000 to 28 000 cm^{-1}. The smallest values are found amongst the hexaaluminates with the magnetoplumbite crystal structure ($D \approx 12\,000$ cm^{-1}) and the (pseudo) perovskites ($D \approx 17\,000$ cm^{-1}). The hexaaluminates have twelvefold anticuboctahedral (acubo) coordination, and the (pseudo) perovskites have (distorted-) cuboctahedral coordination. As shown in Fig. 4 these coordination polyhedra yield very small values for ϵ_{CFS}. The too large centroid shift prevents, however, PCE in perovskites such as $LaAlO_3$. Only the magnetoplumbite $SrAl_{12}O_{19}$, with the smallest redshift (11 050 cm^{-1}) amongst the aluminates, supports PCE. The large abundance of small Al^{3+} cations results in small centroid shift and the coordination around the large Sr^{2+} yields small crystal field splitting. All other aluminates with similar type of coordination such as $LaMgAl_{11}O_{19}$ and $CaAl_{12}O_{19}$ do not support PCE. It demonstrates that the conditions for PCE are very hard to meet in the aluminate compounds.

VII. CONCLUSION

The photon-cascade emission has been demonstrated for $BaSO_4$ and $SrSO_4$, but PCE and df emission appears to occur simultaneously. The possible presence of two different Pr^{3+} sites has been discussed. On the other hand, the $4f5d \rightarrow 4f^2$ emission intensity increases with temperature relative to the $^1S_0$ emission intensity. This suggests a thermal excitation process from the $^1S_0$ state to the $4f5d$ state involving only one Pr^{3+} site.

On excitation into a band between 150–170 nm, SO_4^{2-} complexes are excited that may relax to a self-trapped-exciton-like defect. By means of a resonant energy transfer process Pr^{3+} can be excited to its ^3P_J, $^1I_6$, or $^1D_2$ states. The SO_4^{2-} complexes can also transfer energy directly to the $5d$ states of neighboring Pr^{3+} ions, resulting in $^1S_0$ or df emission. It was demonstrated that the shape of the excitation spectrum of Pr^{3+} in $BaSO_4$, $SrSO_4$, and $CaSO_4$ compare well with that of Ce^{3+}. As a first approximation it is determined by the interaction of the $5d$ electron with the crystal field which is almost the same for Ce^{3+} and for Pr^{3+}.

Trends observed in the relationship between $5d$-level energies of Ce^{3+} and the crystalline environment[22–25] have been briefly summarized and applied to the $4f5d$ states of Pr^{3+}. A set of conditions have been formulated for photon cascade emission by Pr^{3+} to occur in oxides and fluorides. Both crystal field splitting and centroid shift must be small. Tricapped trigonal prismatic and (anti)cuboctahedral type of anion coordination around Pr^{3+} results in small crystal field splitting values ϵ_{CFS}. Fluorides have on average the smallest values for the centroid shift ϵ_c. Centroid shift in the ''complex'' oxides tends to increase with the type of complexes present, in the order SO_4^{2-}, CO_3^{2-}, PO_4^{3-}, BO_3^{3-}, SiO_4^{4-}, to AlO_6^{9-} containing oxides.

The strong bonding between the ligand charge cloud and the cation central to the complexes, such as sulfur in sulfates and boron in borates, results in small centroid shift. At the same time, strong bonding yields high vibrational frequencies and phonon energies that may quench the $^3P_0$ and $^1D_2$ emission in Pr^{3+}, i.e., the second step in the PCE. The internal quantum efficiency of the $^3P_0$ and $^1D_2$ emission in $BaSO_4$ is estimated to be as low as 0.1 and 1 %, respectively. Aluminates and silicates are more favorable with respect to their relatively low phonon energies, but centroid shift tends to be large and chances to observe PCE are small. The silicate $SrBe_2Si_2O_7$ may be an interesting exception.

Although $^1S_0$ emission is observed in $BaSO_4$ and $SrSO_4:Pr^{3+}$, these materials are not interesting from an application point of view. The preferential energy transfer by means of STE's from the host to low lying $4f^2$ states, the presence of $4f5d \rightarrow 4f^2$ emission, and the low quantum efficiency of the $^1D_2$ and $^3P_0$ emission makes these materials highly inefficient phosphors.

ACKNOWLEDGMENTS

The authors wish to thank M. Kirm for his assistance at the SUPERLUMI experimental station. This work was supported by the Netherlands Technology Foundation (STW) and by the IHP-Contract HPRI-CT-1999-00040 of the European Commission.

[1] S. Shionoya and W.M. Yen, *Phosphor Handbook* (CRC press, Boston, 1999).
[2] A. A. Kaminskii, *Laser Crystals, Springer Series in Optical Sciences* (Springer-Verlag, Berlin, 1981), Vol. 14.
[3] A. A. Ballman, S. P. S. Porto, and A. Yariv, J. Appl. Phys. **34**, 3155 (1963).
[4] M. J. F. Digonnet, R. W. Sadowski, H. J. Shaw, and R. H. Pantell, Opt. Fiber Technol.: Mater., Devices Syst. **3**, 44 (1997).
[5] C. D. Marshall, J. A. Speth, S. A. Payne, W. F. Krupke, G. J. Quarles, V. Castillo, and C. Both, J. Opt. Soc. Am. B **11**, 2054 (1994).
[6] T. Jüstel, H. Nikol, and C. R. Ronda, Angew. Chem. Int. Ed. **37**, 3084 (1998).
[7] Shinji Okamoto, H. Kobayashi, and H. Yamamoto, J. Appl. Phys. **86**, 5594 (1999).
[8] P. Dorenbos, M. Marsman, C. W. E. van Eijk, M. V. Korzhik, and B. I. Minkov, Radiat. Eff. Defects Solids **135**, 325 (1995).
[9] C. W. E. van Eijk, P. Dorenbos, and R. Visser, IEEE Trans. Nucl. Sci. **41**, 738 (1994).
[10] M. Laroche, A. Braud, S. Girard, J. L. Doualan, R. Moncorgé, M. Thuau, and L. D. Merkle, J. Opt. Soc. Am. B **16**, 2269 (1999).
[11] S. Nicolast, M. Laroche, S. Girard, R. Moncorge, Y. Guyot, M. F. Joubert, E. Descroix, and A. G. Petrosyan, J. Phys.: Condens. Matter **11**, 7937 (1999).
[12] M. Laroche, M. Bettinelli, S. Girard, and R. Moncorgé, Chem. Phys. Lett. **311**, 167 (1999).
[13] W. W. Piper, J. A. DeLuca, and F. S. Ham, J. Lumin. **8**, 344 (1974).
[14] J. L. Sommerdijk, A. Bril, and A. W. de Jager, J. Lumin. **8**, 341 (1974).
[15] J. L. Sommerdijk, A. Bril, and A. W. de Jager, J. Lumin. **8**, 288 (1974).
[16] A. M. Srivastava and W. W. Beers, J. Lumin. **71**, 285 (1997).
[17] A. M. Srivastava, D. A. Doughty, and W. W. Beers, J. Electrochem. Soc. **143**, 4113 (1996).
[18] A. M. Srivastava, D. A. Doughty, and W. W. Beers, J. Electrochem. Soc. **144**, L190 (1997).
[19] T. Kamegaya, H. Matsuzaki, and M. Yokozawa, IEEE Trans. Electron Devices **25**, 1094 (1978).
[20] P. Dorenbos, J. Lumin. **91**, 91 (2000).
[21] P. Dorenbos, J. Lumin. **91**, 155 (2000).
[22] P. Dorenbos, Phys. Rev. B **62**, 15 640 (2000).
[23] P. Dorenbos, Phys. Rev. B **62**, 15 650 (2000).
[24] P. Dorenbos, Phys. Rev. B **64**, 125117 (2001).
[25] P. Dorenbos, Phys. Rev. B (to be published).
[26] E. van der Kolk, P. Dorenbos, and C.W.E. van Eijk, J. Lumin. (accepted for publication).
[27] R. J. Hill, Can. Mineral. **15**, 522 (1977).
[28] F. C. Hawthorne and R. B. Ferguson, Can. Mineral. **13**, 181 (1975).
[29] F. C. Hawthorne and R. B. Ferguson, Can. Mineral. **13**, 289 (1975).
[30] O. Guillot-Noël, J. T. M. de Haas, P. Dorenbos, and C. W. E. van Eijk, J. Lumin. **85**, 21 (1999).
[31] G. Zimmerer, Nucl. Instrum. Methods Phys. Res. **308**, 178 (1991).
[32] V. G. Plekhanov and V. S. Osminin, Opt. Spectrosc. **39**, 604 (1975).
[33] V. G. Plekhanov and V. S. Osminin, Opt. Spectrosc. **38**, 120 (1975).
[34] B. V. Andrievskii, V. Y. Kurlyak, N. A. Romanyuk, and Z. M. Ursul, Opt. Spectrosc. **66**, 623 (1989).
[35] I. Tokbergenov, E. Feldbach, M. Kerikmäe, A. Lushchic, V. Nagirnyi, T. Nurakhmetov, F. Savkhin, and E. Vasil'chenko, Radiat. Eff. Defects Solids **150**, 495 (1999).
[36] V. G. Shokokh, A. I. Komyak, and N. I. Aleshkevich, Zh. Prikl. Spektrosk. **42**, 400 (1985).
[37] A. R. Lakshmanan, U. Madhusoodanan, B. S. Nair, and D. Sundar, Radiat. Phys. Chem. **51**, 391 (1998).
[38] N. Yamashita, I. Yamamoto, K. Ninagawa, T. Wada, Y. Yamashita, and Y. Nakao, Jpn. J. Appl. Phys. **24**, 1174 (1985).
[39] A. P. Vink, E. van der Kolk, P. Dorenbos, and C. W. E. van Eijk, J. Alloys Compd. (to be published).
[40] A. R. Lakshmanan, Prog. Mater. Sci. **44**, 1 (1999).
[41] L. H. Brixner, M. K. Crawford, and G. Blasse, J. Solid State Chem. **85**, 1 (1990).
[42] J. M. F. van Dijk and M. F. H. Schuurmans, J. Chem. Phys. **78**, 5317 (1983).
[43] R. Balda, J. Fernández, I. Saéz de Ocáriz, M. Voda, A. J. García, and N. Khaidukov, Phys. Rev. B **59**, 9972 (1999).
[44] M. Malinowski, W. Woliński, R. Wolski, and W. Strek, J. Lumin. **48-49**, 235 (1991).
[45] H. Dornauf and J. Heber, J. Lumin. **22**, 1 (1980).
[46] A. Lorenzo, L. E. Bausá, and J. García Solé, Phys. Rev. B **51**, 16 643 (1995).
[47] R. C. Naik, N. P. Karanjikar, and M. A. N. Razvi, J. Lumin. **54**, 139 (1992).
[48] A. Ellens, A. Meijerink, and G. Blasse, J. Lumin. **59**, 293 (1994).
[49] B. Tanguy, P. Merle, M. Pezat, and C. Fouassier, Mater. Res. Bull. **9**, 831 (1974).
[50] A. Meijerink, J. Nuyten, and G. Blasse, J. Lumin. **44**, 19 (1989).
[51] R. Visser, P. Dorenbos, C. W. E. van Eijk, A. Meijerink, G. Blasse, and H. W. den Hartog, J. Phys.: Condens. Matter **5**, 1659 (1993).
[52] J. C. van 't Spijker, P. Dorenbos, C. W. E. van Eijk, K. Krämer, and H. U. Güdel, J. Lumin. **85**, 1 (1999).
[53] M. Laroche, J. L. Doualan, S. Girard, J. Margerie, and R. Moncorgė, J. Opt. Soc. Am. B **17**, 1291 (2000).
[54] M. F. Reid, L. van Pieterson, R. T. Wegh, and A. Meijerink, Phys. Rev. B **62**, 14 744 (2000).
[55] E. van der Kolk, P. Dorenbos, and C.W.E. van Eijk, Opt. Commun. **197**, 317 (2001).
[56] E. van der Kolk (unpublished).
[57] E. van der Kolk, P. Dorenbos, and C.W.E. van Eijk, J. Phys.: Condens. Matter. **13**, 1 (2001).
[58] J. M. P. J. Verstegen and J. L. Sommerdijk, J. Lumin. **9**, 297 (1974).